Single-vortex-induced voltage steps in Josephson-junction arrays

1997 J. Phys.: Condens. Matter 9 1813

(http://iopscience.iop.org/0953-8984/9/8/011)

J. Phys.: Condens. Matter **9** (1997) 1813–1829. Printed in the UK PII: S0953-8984(97)78913-6

Single-vortex-induced voltage steps in Josephson-junction arrays

P H E Tiesinga†, T J Hagenaars†‡, J E van Himbergen† and Jorge V José§

† Instituut voor Theoretische Fysica, Princetonplein 5, Postbus 80006, 3508 TA Utrecht, The Netherlands

‡ Institut für Theoretische Physik, Universität Würzburg, Am Hubland, 97074 Würzburg, Germany

§ Department of Physics and Center for Interdisciplinary Research on Complex Systems, Northeastern University, Boston, MA 02115, USA

Received 24 October 1996, in final form 13 December 1996

Abstract. We have numerically and analytically studied (ac + dc)-driven Josephson-junction arrays with a single vortex or with a single vortex–antivortex pair present. We find single-vortex steps in the voltage versus current (I–V) characteristics of the array. They correspond microscopically to a single vortex phase-locked to move a fixed number of plaquettes per period of the ac driving current. In underdamped arrays we find vortex motion period doubling on the steps. We observe subharmonic steps in both underdamped and overdamped arrays. We successfully compare these results with a phenomenological model of vortex motion with a non-linear viscosity. The I–V characteristic of an array with a vortex–antivortex pair displays fractional voltage steps. A possible connection of these results to present-day experiments is also discussed.

1. Introduction

The presence of giant Shapiro steps and giant fractional Shapiro steps in the I–V characteristics of 2-D Josephson-junction arrays has attracted significant attention recently [1–7]. These 2-D arrays may be of use as a source of coherent microwave radiation [8]. In a separate context the flux-flow dynamics of vortices has been studied [9–11]. The reported experimental observation of ballistic vortex motion [12] has also stimulated further theoretical and numerical investigations [13–17] of the mass and friction of a vortex in an array. Until now these numerical investigations have focused on dc-driven vortices. In this work we perform numerical simulations on Josephson-junction arrays, with only one vortex or with a vortex–antivortex pair present in it, driven by a time-dependent current $i(t) = i_{dc} + i_{ac}\cos(2\pi\nu t)$. We calculate the voltage V versus i_{dc} (i.e., I–V) characteristics. We find harmonic and subharmonic single-vortex voltage steps and analyse the underlying phase-locked vortex motion. A vortex–antivortex pair separated by a distance Δx along the direction of the injected external current phase-locks onto fractional voltage steps.

The arrays are 2-D lattices of superconducting islands (sites) connected by Josephson junctions (bonds). The unit cells (plaquettes) of these lattices can be, for example, square or triangular. The vortices are represented by eddy-current patterns about a plaquette. Here we consider the classical regime defined by $E_J \gg E_c = e^2/2C$, where E_J is the Josephson coupling energy and E_c the charging energy of two islands, e the electron charge, and C

0953-8984/97/081813+17$19.50

the capacitance of a junction. In this regime quantum fluctuations are neglected, leaving the phases $\theta(\boldsymbol{r})$ of the Ginzburg–Landau order parameter on the islands as the only dynamical variables.

In this case the array is well modelled by the resistively capacitively shunted junction (RCSJ) model, defined by the total bond current $i(\boldsymbol{r}, \boldsymbol{r}')$ between nearest-neighbour sites $\boldsymbol{r}$ and $\boldsymbol{r}'$:

$$i(\boldsymbol{r}, \boldsymbol{r}') = \beta_c \ddot{\theta}(\boldsymbol{r}, \boldsymbol{r}') + \dot{\theta}(\boldsymbol{r}, \boldsymbol{r}') + \sin[\theta(\boldsymbol{r}, \boldsymbol{r}') - 2\pi A(\boldsymbol{r}, \boldsymbol{r}')] \tag{1}$$

plus Kirchhoff's current-conservation conditions at each site. Here the dots represent time derivatives. The three contributions to $i(\boldsymbol{r}, \boldsymbol{r}')$ are the displacement, and the dissipative and the superconducting currents, respectively. The phase difference across a junction is $\theta(\boldsymbol{r}, \boldsymbol{r}') \equiv \theta(\boldsymbol{r}) - \theta(\boldsymbol{r}')$. The currents are expressed in units of the junction critical current I_c; time is measured in units of the characteristic time $1/\omega_c = \hbar/(2eR_nI_c)$, and $\beta_c = (\omega_c/\omega_p)^2$ is the Stewart–McCumber parameter [20], with the plasma frequency ω_p defined as $\omega_p^2 = 2eI_c/\hbar C$, and R_n is the junction's normal-state resistance. The bond frustration variable $A(\boldsymbol{r}, \boldsymbol{r}')$ is defined as the line integral of the vector potential $\boldsymbol{A}$:

$$A(\boldsymbol{r}, \boldsymbol{r}') = \frac{1}{\phi_0} \int_{\boldsymbol{r}}^{\boldsymbol{r}'} \boldsymbol{A} \cdot \mathrm{d}\boldsymbol{l} \tag{2}$$

with the elementary quantum of flux $\phi_0 = h/2e$. The frustration parameter f measures the average flux piercing a plaquette, measured in units of ϕ_0.

The motivation for this paper is twofold: to study the dynamics of a few vortices in an array, and to see whether the results can be generalized in order to explain dynamical non-equilibrium states, like the axisymmetric coherent vortex state [6]. Here we deal mainly with the analysis of single-vortex voltage steps. The motion of a vortex produces a Faraday voltage across the array. In this paper we find three types of new step. First we find single-vortex voltage steps. The voltage V on these steps is proportional to an integer multiple n of the frequency of the ac drive:

$$V = \frac{nh\nu}{2e} \qquad n = 0, 1, 2, \ldots. \tag{3}$$

In the following we will also consider natural units $\hbar/2e = 1$. Then the voltage is normalized such that it corresponds to 2π times the number of jumps between plaquettes of the vortex per time unit. This differs from another often-used normalization by a factor N_y, the number of junctions perpendicular to the direction of the current injection. On such a step the motion of the single vortex is phase-locked to move an integer number of plaquettes per period $1/\nu$. Next we find subharmonic single-vortex steps in the I–V characteristics of both overdamped and underdamped arrays. On these steps the voltage is

$$V = \frac{n}{m}\frac{h\nu}{2e} \qquad n = 0, 1, 2, \ldots \qquad m = 1, 2, \ldots. \tag{4}$$

The dynamics on these steps corresponds to the vortex moving n plaquettes in m periods.

Finally we simulate a vortex–antivortex pair and obtain the following steps:

$$V = \frac{nN_y}{m}\frac{h\nu}{2e} \qquad n = 0, 1, 2, \ldots \qquad m = 1, 2, \ldots. \tag{5}$$

Each vortex moves $nN_y/2$ plaquettes every m periods.

These new steps should be contrasted with other types of step that arise in Josephson-junction arrays. In single junctions, harmonic ($V = nh\nu/2e$) voltage steps are present in both experimentally and numerically obtained I–V characteristics [21]. These steps are called single-junction Shapiro steps. On these steps the single junction has n phase-slips per

period $1/\nu$. In simulations of and experiments on (ac + dc)-driven arrays, so-called giant Shapiro steps have been observed [1–3]. On these steps the $N_x N_y$ individual junctions along the direction of the external current are all phase-locked on the same single-junction Shapiro step, and one obtains

$$V = N_x N_y \frac{nh\nu}{2e} \qquad n = 0, 1, 2, \ldots.$$

The harmonic and subharmonic single-vortex voltage steps are therefore small in comparison to the giant Shapiro steps. Subharmonic giant Shapiro steps are observed experimentally [3] and in simulations [6, 7]. A particular example of these half-integer steps is found in the axisymmetric coherent vortex states (ACVS). These stationary states correspond to an oscillating pattern of vortex and antivortex streets, which arrange themselves at a well-defined angle with respect to the current direction [6].

In studies of and experiments on (ac + dc)-driven arrays, with an average rational flux $(p/q)\phi_0$ piercing through each plaquette, giant *fractional* Shapiro steps were observed [2, 4, 5]. On these steps the voltage is

$$V = \frac{N_x N_y}{q} \frac{nh\nu}{2e} \qquad n = 0, 1, 2, \ldots.$$

An explanation for such steps has been proposed and verified in simulations [2, 4]: an $f = p/q$ array has q degenerate ground states, consisting of vortex lattices, carried into each other by translations. In one period of the driving current the vortex lattice moves from one degenerate state to the next. After q periods every vortex has moved through the whole array, generating the observed voltage.

This shows that there are two kinds of Shapiro step in Josephson-junction arrays. Those based on the coherent phase-slips of all of the individual junctions in the array (giant Shapiro steps) and those involving coherent oscillatory vortex motions (giant fractional Shapiro steps and ACVS).

The approach of our study is to have only one vortex, which makes it is possible to separate the generic effect of vortex motion from the effects of interaction between them. One can systematically study the underlying microscopic dynamics of the phase-locked vortex motion. Then by considering a vortex–antivortex pair one can study the effect of interaction in its simplest form on the phase-locked states. The vortex dynamics on single-vortex voltage steps has a number of new and interesting features, e.g. we observe vortex motion with period doubling in underdamped arrays. The underlying microscopic vortex motion repeats itself only after 2, 4, 8, or even 16 periods $1/\nu$, although the vortex still moves, on average, a fixed number of plaquettes per period. In this paper we discuss how these steps can observed experimentally in arrays with a low density of vortices.

Previous authors [9, 10, 17] have studied simple models of vortex motion. In these models the vortex is described as a point particle of mass $M(\beta_c)$ experiencing a certain friction, and moving in a sinusoidal potential. In reference [17] we found that the I–V characteristic of a dc-driven array in the vortex regime is well described by such a vortex equation of motion in terms of the vortex coordinate y containing, instead of the usual linear viscous force, a non-linear one:

$$M(\beta_c)\ddot{y} + \frac{A(\beta_c)\dot{y}}{1 + B(\beta_c)|\dot{y}|} + i_0 \sin 2\pi y = i. \tag{6}$$

In this equation $A(\beta_c)$ and $B(\beta_c)$ are phenomenological parameters. This analysis is similar in spirit to the description of long Josephson junctions in terms of the fluxon coordinates [18]. An interesting question previously left unaddressed, and considered in this paper,

is whether a phenomenological model for the vortex coordinate can still reproduce the I–V characteristic of an (ac + dc)-driven array. In this work we resolve this question and we compare the I–V characteristic of an array with the result of equation (6) with a time-dependent current $i = i_{dc} + i_{ac}\cos 2\pi\nu t$, and using the parameters $M(\beta_c)$, $A(\beta_c)$ and $B(\beta_c)$ obtained for dc-driven arrays. The results of equation (6) and the simulations are in reasonable agreement over a broad range of values of the frequency and the amplitude of the ac drive. In other words the vortex experiences a non-linear friction in an (ac + dc)-driven array.

The outline of the paper is as follows. In section 2 we discuss the calculational algorithm for computing the I–V characteristic. In section 3 we present the I–V characteristics containing the harmonic and subharmonic single-vortex steps and discuss the possibility of experimental verification. We then study subharmonic single-vortex voltage steps and period-doubled vortex motion using the microscopic current distribution in the array as a function of time. Finally we compare the result of equation (6) to those of the I–V characteristics obtained from the Josephson-junction array simulations. In section 4 we investigate the effects of interaction and discuss the vortex–antivortex voltage steps in the I–V characteristic. In section 5 we present our conclusions.

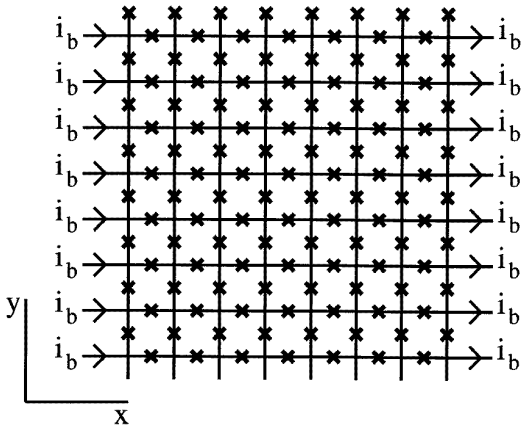

Figure 1. The array geometry used in the simulations, illustrated with an 8×8 array. Junctions are denoted as crossed bonds. Periodic boundary conditions are imposed in the y-direction, while the current bias i_b is applied along the x-direction.

2. Calculational approach

We numerically solve the equations of motion for a two-dimensional array. We show the square lattice of $L_x \times L_y$ sites in figure 1. The sites are connected through Josephson junctions, denoted by crosses. We use the RCSJ model of equation (1) to relate the current $i(\boldsymbol{r}, \boldsymbol{r}')$ through the Josephson junction to the phase difference $\theta(\boldsymbol{r}, \boldsymbol{r}')$. We use periodic boundary conditions (PBC) in the y-direction, while the current is fed in and taken out along the x-direction. This set of coupled non-linear differential equations can be integrated efficiently using a fast-Fourier-transform algorithm [6, 22]. The array consists of $N_x \times N_y$

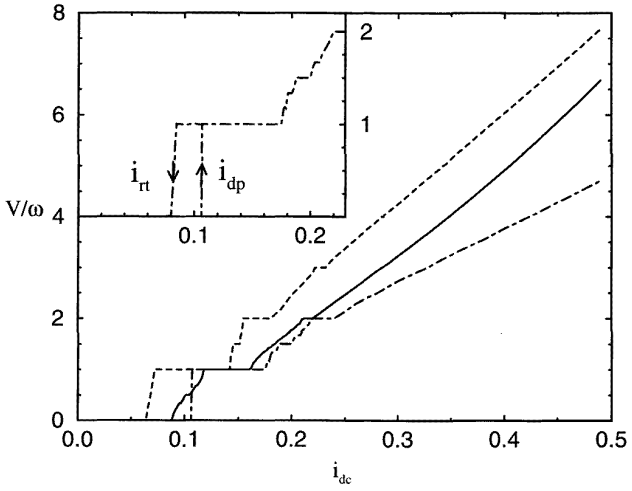

Figure 2. I–V characteristics obtained from simulation of a 16×32 array with the parameters: $i_{ac} = 0.10$, $\nu = \frac{1}{25}$ and $\beta_c = 0$ (continuous line); $\nu = \frac{1}{50}$ and $\beta_c = 5$ (dotted line); and $\nu = \frac{1}{50}$ and $\beta_c = 20$ (chain line). The voltage in natural units is normalized by $\omega = 2\pi\nu$. The inset contains a close-up of the $\beta_c = 20$ curve, with an added I–V branch showing hysteresis.

plaquettes ($N_x = L_x - 1$ and $N_y = L_y$). The vorticity $n(\boldsymbol{R})$ is defined as

$$2\pi n(\boldsymbol{R}) = 2\pi f + \sum_{\mathcal{P}(\boldsymbol{R})} (\theta(\boldsymbol{r}, \boldsymbol{r}') - 2\pi A(\boldsymbol{r}, \boldsymbol{r}')). \tag{7}$$

Here $\mathcal{P}(\boldsymbol{R})$ denotes an anticlockwise sum around the plaquette $\boldsymbol{R}$, and the gauge-invariant phase difference $\theta(\boldsymbol{r}, \boldsymbol{r}') - 2\pi A(\boldsymbol{r}, \boldsymbol{r}')$ is taken between $-\pi$ and $+\pi$.

We are interested in the behaviour of vortices in Josephson-junction arrays. Stable vortices can be explicitly introduced in the initial phase configuration by the application of a small frustration [17]. The plaquette coordinate $\boldsymbol{R}$ with unit vorticity will be called the topological vortex coordinate. The voltage $V(t)$ is obtained from

$$V(t) = \sum_{y=0}^{L_y - 1} \frac{\mathrm{d}}{\mathrm{d}t} [\theta(L_x - 1, y) - \theta(0, y)]. \tag{8}$$

The time average of $V(t)$ is related to the average vortex velocity $v = V/2\pi$. The microscopic dynamics of the vortex motion is reflected in the eddy-current distribution $C(\boldsymbol{R}, t)$:

$$C(\boldsymbol{R}, t) = \sum_{\mathcal{P}(\boldsymbol{R})} i(\boldsymbol{r}, \boldsymbol{r}', t) \tag{9}$$

where $\mathcal{P}(\boldsymbol{R})$ is the anticlockwise sum over bonds about a dual lattice site $\boldsymbol{R}$. The vortex shows up as a local extremum in the eddy-current distribution.

3. Single-vortex-induced voltage steps

In this section we present the results of our simulations of a single vortex in a Josephson-junction array. In the first subsection we discuss results for the I–V characteristics. In the

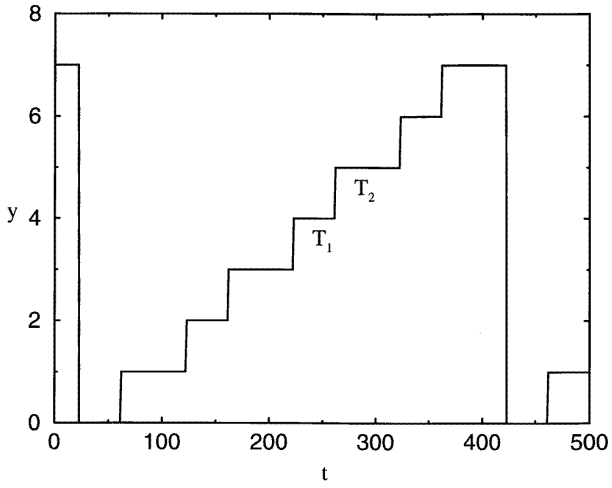

(a)

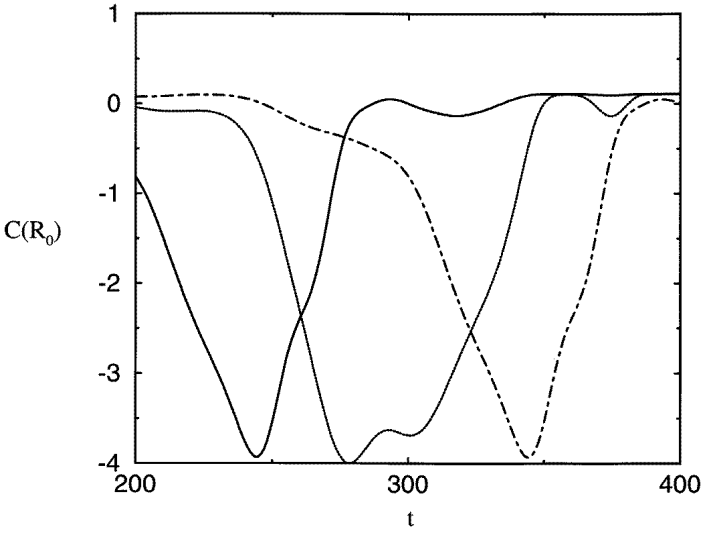

(b)

Figure 3. Period doubling on the $n = 1$ step. The results are obtained from a simulation of an 8×8 array, with the parameters $\beta_c = 25$, $\nu = 1/50$, $i_{ac} = 0.10$, and $i_{dc} = 0.13$. In (a) we plot the vortex position versus time. In (b) we plot the eddy currents versus time at three adjacent plaquettes of the middle column. The continuous, dotted and chain lines are respectively the first, second and third plaquette in the middle column of the array. The minima in these graphs indicate the positions of the vortex.

next subsection a detailed description of the single-vortex voltage steps is given. We discuss the microscopic vortex motion, including its period doubling and the subharmonic single-vortex voltage steps. This is followed by a comparison of a simple model for vortex motion to the simulation results, and finally the discussion of possible experimental verification.

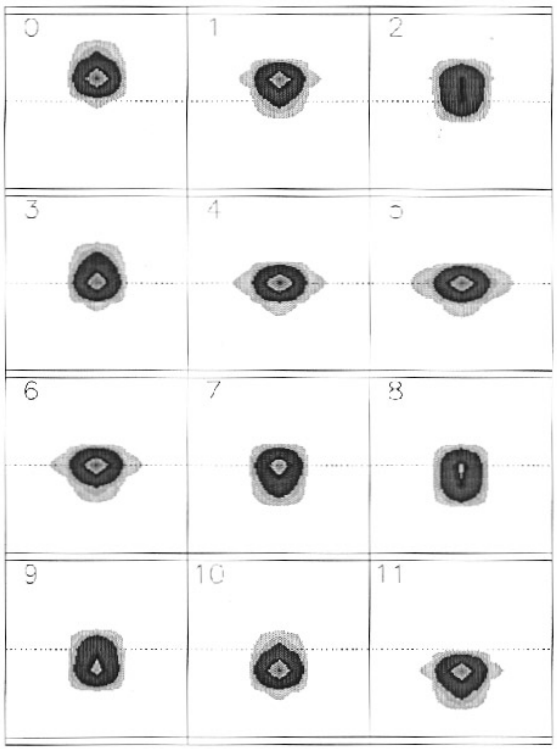

Figure 4. Period doubling on the $n = 1$ step. The parameters are the same as in figure 3. We show snapshots of the eddy-current distributions at different times. The time step between two snapshots is 10 (in units of $1/\omega_c$). The eddy-current distributions are smoothed out by interpolation.

3.1. The I–V characteristics

The I–V characteristics are generated by gradually increasing the bias current i_{dc} from 0 starting with an initial configuration containing a vortex. We express the voltage in natural units $\hbar/2e \equiv 1$ and normalized by the frequency $2\pi\nu$. The harmonic steps then occur at integer voltage values.

For currents below the depinning current i_{dp} the voltage is zero (see figure 2), when it is averaged over enough periods of the ac drive. The vortex deforms in response to the ac + dc drive, but stays in the same plaquette [23]. Or, for low enough frequency ν and large enough i_{ac}, it can even oscillate back and forth over a finite number of plaquettes.

The second branch of the I–V characteristic is generated by decreasing the bias current. As the initial phase configuration one uses the final phase configuration obtained in the upward sweep. At the retrapping current i_{rt} the average voltage returns to zero. In underdamped arrays the retrapping current i_{rt} can be different from i_{dp}. This hysteretic behaviour has often been interpreted as evidence for inertia of the vortex in the dc-driven case. An example of hysteresis is shown in the inset of figure 2. Focusing the discussion on the upward current sweep we encounter the first plateau at $V = 2\pi\nu$. This is the first single-vortex step. The vortex moves on average one plaquette per period. There are two

more steps visible at multiples of $2\pi\nu$ in figure 2. Above $i_{dc} \approx 0.25$ no steps are visible any more. The step width has become smaller than the current grid size $\Delta i_{dc} = 0.01$. The $\beta_c = 0$ I–V characteristic exhibits a pronounced upward curvature. Hence the vortex viscosity is non-linear [17]. Between the $n = 1$ and $n = 2$ steps a small subharmonic step, at $V/2\pi\nu = \frac{3}{2}$, is visible in figure 2. On this step the vortex moves three plaquettes every two periods. Using a smaller $\Delta i_{dc} = 0.002$ one can even observe the $\frac{4}{3}$ and $\frac{5}{3}$ steps.

Increasing the damping parameter β_c, for given ν, shifts the steps to higher values of the current bias i_{dc}. This is due to an increase in the vortex viscosity with β_c [17]. When β_c is changed from 5 to 20, the $n = 3$ step width is gradually reduced to below the current grid size $\Delta i_{dc} = 0.01$. For $\nu > 1.0$ no integer steps are present any more. For these frequencies the velocity for which the vortex would phase-lock on the first integer step lies above the maximum vortex velocity in the array.

The width of a particular step varies in an oscillatory fashion as a function of $i_{ac}/2\pi\nu$. This is qualitatively similar to the step width behaviour of a single junction, which varies as a Bessel function of i_{ac}. By adjusting i_{ac} one can make more steps visible.

Table 1. The periodicity of the voltage v_p averaged over one period of the driving force as a function of i_{dc}. The data are obtained from simulations of an 8×8 array, with the parameters $\beta_c = 25$, $\nu = 1/50$, and $i_{ac} = 0.10$.

I_{dc}	Step	Period
0.0–0.06	$n = 0$	1
0.075		2
0.08		4
0.085		8
0.088		16
0.09		~ 24
0.095		8
0.10		4
0.105, 0.11		2
0.115		1
0.125	$n = 1$	4
0.13–0.155		2
0.165–0.19		1

3.2. Single-vortex-induced voltage steps

We now turn to the microscopic vortex motion on the single-vortex voltage steps. We first consider the $n = 0$ step, i.e. the response of a vortex that is pinned in one plaquette. One may expect the response to have the same period as the ac drive. In that case the quantity v_p, the voltage averaged over one period of the drive, is constant and equal to zero. We find, however, that v_p can be non-zero on the $n = 0$ step. This is repeated periodically in time. In table 1 we show the periodicity of v_p (in units of the driving period) as a function of i_{dc} for an 8×8 array with the parameters $\beta_c = 25$, $\nu = 1/50$, $i_{ac} = 0.1$.

Next we focus on the $n = 1$ step in table 1. The vortex depins at $i_{dc} \approx 0.12$. For $i_{dc} = 0.13$ the voltage v_p alternates between two different values. Figures 3 and 4 show the corresponding vortex motion. Figure 3(a) shows the topological vortex coordinate, defined in equation (7), versus time. It shows that the time the vortex spends at one plaquette alternates between two values T_1 and T_2. The sum $T_1 + T_2$ is equal to $2/\nu$. In figure 3(b)

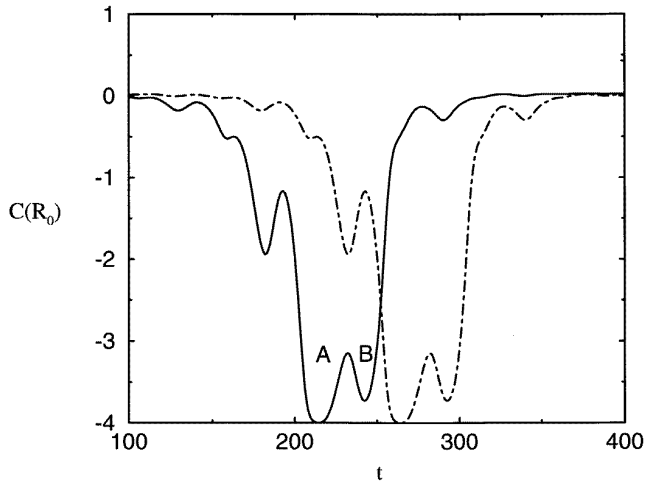

Figure 5. Vortex motion on a $\frac{1}{2}$ step for an 8×32 array, with the parameters $\beta_c = 0$, $\nu = 1/25$, $i_{ac} = 0.10$, and $i_{dc} = 0.11$. We plot the eddy current versus time, as in figure 3(b), for two adjacent plaquettes (denoted by the continuous and the chain lines respectively). The minima A and B in this graph indicate the positions of the vortex.

we plot the eddy currents of three adjacent plaquettes versus time. In figure 4 we show snapshots of the spatial distribution of eddy currents. Frames 0 and 10 are almost equivalent. A jump occurs between frames 2 and 3 and between frames 8 and 9. The difference between T_1 (frames 0–2) and T_2 (frames 3–8) is clearly visible. All of the figures show that the actual vortex motion is periodic with twice the period of the driving force.

Subharmonic steps turn out to be a generic feature of the I–V characteristics of (ac+dc)-driven arrays. They are observed for different values of i_{ac}, ν, β_c and system sizes. Many different voltage values are possible. We studied a $\frac{1}{2}$ step in detail. At $i_{dc} = 0.11$ we found an $n = \frac{1}{2}$ step in a $\beta_c = 0$, $\nu = 1/25$, 8×32 array. On this step the generic behaviour is as follows. Although the vortex deforms significantly during the first period, the topological vortex coordinate does not change. Only in the second period does it jump to the neighbouring plaquette. We now describe a typical example. In figure 5 we show the eddy current versus time of the plaquette containing the vortex. Both curves have two minima: A and B. In minimum B the vortex has a different shape (and hence feels a different potential) to that in A. From this we can deduce the following scenario. During the first period the vortex deforms from configuration A to B, staying in the same plaquette. In the following period it jumps to the next plaquette into the adjacent minimum A. We also found a case ($i_{dc} = 0.072$, $\nu = 1/50$) in which the vortex briefly jumped to the next plaquette (and returned to the original plaquette) during the first period.

3.3. Comparison to a phenomenological model of vortex motion

In this subsection we compare the results of the numerical simulations to the results of a simple model for the vortex motion. The motion of a single vortex in an array can be modelled by that of a point particle with mass M that, driven by a (Lorentz) force i, moves through a sinusoidal pinning potential and experiences a linear viscous damping force with

constant viscosity coefficient η [9, 10]. The vortex mass M can be calculated by equating the electromagnetic energy stored in the array to a vortex kinetic energy $\frac{1}{2}M\dot{y}^2$. The friction can be determined by equating the dissipated energy to $\eta\dot{y}^2$. This results in the following equation of motion for position $y(t)$, generalized to include a time-dependent driving force i:

$$\pi\beta_c\ddot{y} + \pi\dot{y} + i_0 \sin 2\pi y = i_{dc} + i_{ac}\cos 2\pi\nu t. \tag{10}$$

For a square array $i_0 \approx 0.10$ [9]. Every time the particle moves one plaquette ($y \to y+1$), an integrated 2π voltage pulse is generated across the array in the x-direction. The average of $2\pi\dot{y}$ is then the dimensionless average voltage measured across an array.

We recently introduced a modified vortex equation of motion [17] for dc-driven vortices, including a non-linear viscosity

$$M(\beta_c)\ddot{y} + \frac{A(\beta_c)\dot{y}}{1 + B(\beta_c)|\dot{y}|} + i_0 \sin 2\pi y = i_{dc} + i_{ac}\cos 2\pi\nu t. \tag{11}$$

The parameter values for overdamped case are $M(\beta_c) = 0$, $A \approx 2.7$, $B \approx 1.8$, and $i_0 = 0.1$ [17].

Equations (10) and (11) are similar to the equations describing single Josephson junctions. To connect to the single-Josephson-junction literature, replace y by a phase $\theta = 2\pi y$, divide by i_0 and absorb the coefficient in front of the first derivative of θ in a new time unit:

$$\beta\ddot{\theta} + \frac{\dot{\theta}}{1 + \mathcal{B}\dot{\theta}} + \sin\theta = \bar{i}_{dc} + \bar{i}_{ac}\cos\Omega\tau \tag{12}$$

where

$$\beta = M(\beta_c)\frac{i_0 2\pi}{A^2} \qquad \mathcal{B} = \frac{i_0}{A}B \qquad \Omega = \nu\frac{A}{i_0} \qquad \bar{i}_{ac} = \frac{i_{ac}}{i_0} \qquad \bar{i}_{dc} = \frac{i_{dc}}{i_0}.$$

To allow for a more quantitative comparison we use the procedure described in reference [17] to find the parameters A and B in equation (11). That is, we fit the I–V curve in the dc-driven case to the form

$$\frac{\sqrt{i_{dc}^2 - i_0^2}}{A - B\sqrt{i_{dc}^2 - i_0^2}}.$$

Given these parameters one can numerically calculate the I–V relationship predicted by equation (11). In figure 6 we compare these results for one specific set of values i_{ac}, ν and β_c to the I–V characteristic obtained from simulations of the full array. The results of equation (11) are in good agreement with the simulation for larger currents $i_{dc} > 0.3$. For this current regime the steps are too small with respect to the current grid $\Delta i_{dc} = 0.01$ to be visible.

For lower currents the agreement is less satisfactory. The steps in the simulations and in equation (11) do overlap to a large extent, but the lower edge of the steps is underestimated by equation (11), especially at depinning. However, one finds large deviations when comparing the simulation data to equation (10), the model with linear viscosity.

The phenomenological vortex mass for $\beta_c < 35$ is $M(\beta_c) = 0$, as found from the dc I–V curves in reference [17]. In the dc + ac case, however, we find small hysteresis loops in the I–V characteristics. One could interpret this as an indication for the presence of a non-zero $M(\beta_c)$. The hysteretic behaviour of equation (11) is complicated. Using a different $M \neq 0$ with the computed values of $A(\beta_c)$ and $B(\beta_c)$ did not yield better agreement with the simulation results.

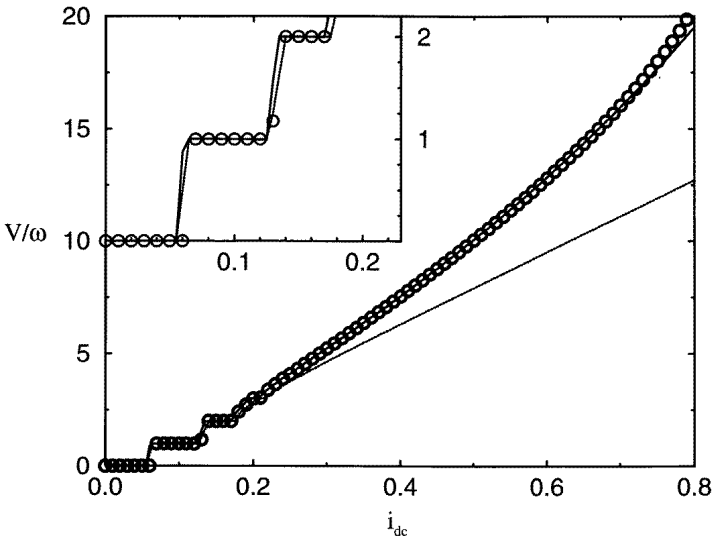

Figure 6. A comparison of results obtained using the model equation (12) (dotted line; parameters: $\Omega = \pi/5$, $\beta = 0.4$, and $\bar{i}_{ac} = 1.0$) and (full line; parameters: $\Omega = 0.617$, $\mathcal{B} = 0.0424$, $\beta = 0$, and $\bar{i}_{ac} = 1.0$) to the simulations of the full 16×32 array (circles; $\nu = \frac{1}{50}$, $\beta_c = 2$, and $i_{ac} = 0.10$).

3.4. Experimental verification

In order to see how the single-vortex phase-locking mechanism would manifest itself in experimentally accessible conditions, we now reinstate physical dimensions using experimental parameters [24]. Typical values for the parameters are $I_c = 0.01$–2.0 μA, $I_c R_n = 300$ μV, $\omega_c = 2eR_n I_c/\hbar \sim 1$ GHz and $\beta_c = 10$–100. The single-vortex voltage steps would occur for $i_{dc} = 0.10$–0.30 I_c and for frequencies $\nu < 0.10\,\omega_c \sim 100$ MHz, and $\beta_c < 50$.

Experiments are conducted at a finite temperature. Voltage steps are observed as a reduction in the differential resistance $\mathrm{d}V/\mathrm{d}I$, while at zero temperature $\mathrm{d}V/\mathrm{d}I = 0$ on a step. This reduction should be large enough, and extend over a sufficiently large current range, in order to be measurable. The temperature is expressed in units of $T_0 = \hbar I_c/2ek_B \approx 2 \times 10^7\, I_c$. We have performed a $T \neq 0$ simulation for one particular case: a 16×16 array with the parameters $\nu = \frac{1}{25}$, $\beta_c = 0$, and $i_{ac} = 0.10$. The simulation was done using the algorithm introduced in reference [25], as extended for arrays [6]. We found that up to $T = 0.004\,T_0$ the $n = 1$ step was clearly visible. For $T = 0.008\,T_0$ a reduction in $\mathrm{d}V/\mathrm{d}I$ was hardly discernible. This puts an upper bound on the appropriate temperatures, varying from $T = 1$ to 200 mK with the value of I_c.

To study the single-vortex phase-locking phenomena experimentally, one can use relatively small samples, to make sure that only a small absolute number of vortices are present at any time, or a large array with a low vortex density. In the former type of experiment the interaction of the vortex with the boundaries, or equivalently with image antivortices, has to be taken into account. When moving to a boundary, a vortex may either escape from the array or reflect as an antivortex [19]. In the parameter regime studied in this paper, vortices are entering the array and leaving it again at the opposite boundary.

In practice the small number of vortices present will therefore fluctuate slightly. This may affect the way in which phase-locking is established as compared to our simulation in which only one vortex is present at any time. To estimate this effect we have simulated a finite array in a small magnetic field and also found steps in the I–V characteristics due to phase-locking with the ac drive at voltages slightly different from those mentioned above.

We also have performed simulations of triangular arrays, often used experimentally, and find qualitatively the same scenario for the occurrence of single-vortex voltage steps, as reported in section 3.1.

4. Vortex–antivortex-pair-induced steps

In this section we consider the effect of vortex–antivortex interaction on the single-vortex voltage steps. In the first subsection we show the fractional voltage steps in the I–V characteristic due to the vortex–antivortex interaction, and obtain these steps from a phenomenological model for vortex motion including the logarithmic interaction. In the second subsection we briefly discuss the analogous behaviour of excess and missing vortices in a checkerboard ground state of an $f = \frac{1}{2}$ array.

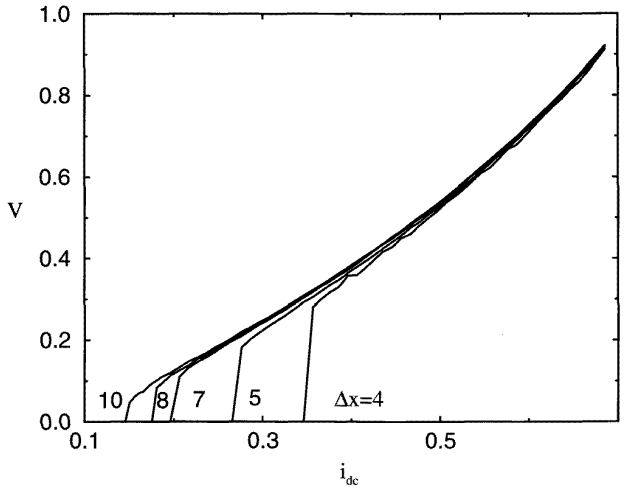

Figure 7. The I–V characteristic of a vortex and an antivortex separated by the distances $\Delta x = 4$, 5, 7, 8, and 10 in an overdamped dc-driven 32×32 array. The annihilation current is the current at which the average voltage drops to zero in the I–V characteristic of the downward current sweep.

4.1. A vortex–antivortex pair in an $f = 0$ array

We calculate the zero-temperature I–V characteristics of an array containing a vortex–antivortex pair. There is no applied magnetic field, and the pair is included in the initial configuration by construction [17]. In order to show how one may obtain meaningful results starting from such a metastable configuration, let us first discuss the case of only a dc drive. When the applied current is zero, the only mechanism that may prevent the annihilation of the pair is the pinning of the lattice. Pinning will prevent annihilation if the mutual

separation is at least eight lattice constants. This minimum distance is in approximate agreement with the value of 0.10 [9] (in units of the junction critical current) for the maximum pinning force on a vortex in an infinite system. However, when the current is non-zero, and the vortices move in different rows (in opposite directions), annihilation may be absent even when the perpendicular distance between the rows is less than eight lattice constants, depending on the magnitude of the current. We have studied this stabilization by the driving force quantitatively by performing downward current sweeps starting from a number of initial configurations containing pairs with different separation distances Δx. The I–V characteristics are shown in figure 7. When the pair is unstable, and thus annihilated, the average voltage obtained from the simulations sharply drops to zero. This annihilation current strongly depends on the separation distance of the pair in the initial configuration. A higher current is needed to stabilize a smaller pair.

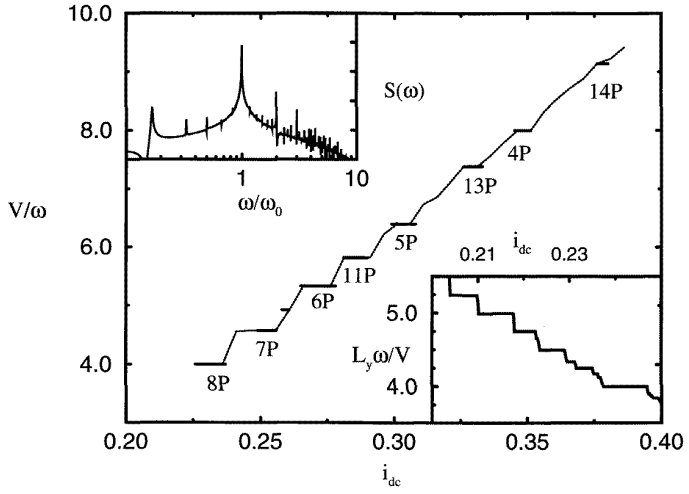

Figure 8. The I–V characteristic of a vortex–antivortex pair with the separation distance $\Delta x = 7$ in an overdamped 32×32 array. The ac component of the driving current has frequency $\nu = \frac{1}{25}$ and amplitude $i_{ac} = 0.10$. The labels mP signify the underlying periodicity of the motion on these steps (i.e. the m in equation (5)). In the upper inset we show the spectral function of the voltage for the 6P step. In the lower inset we show the I–V characteristic obtained from the model for vortex–antivortex-pair motion in the text. We used the following parameters: $L_y = 32$, $2\pi\nu = 1.186$, $\mathcal{B} = 0.0674$, and $\Delta x = 8$. Here we plot, instead of V, $L_x\omega/V$. Steps then arise at the values m/n. The higher n, the smaller the step width.

Next we consider the behaviour of an (ac + dc)-driven pair. Since two vortices move in opposite directions under the influence of the current, their mutual distance will change in time. Phase-locking can therefore not be established for a voltage corresponding to one jump per period, since in the next period the environment has changed, and thereby the interaction strength. We nevertheless find steps in the I–V characteristics of these systems. Once the vortex and the antivortex have traversed $L_y/2$ plaquettes, they cross each other again because we have periodic boundary conditions. Phase-locking is established if at that point the phases are the same again. If phase-lock is established over n traversals, and the motion is periodic with period m (in units of the external frequency ν), then the observed voltage is: $V = nL_y/m2\pi\nu$. We can find each of these steps in the I–V characteristic in figure 8, although for higher n the step width decreases rapidly. The step width is typically

small ($\sim$0.01).

When the vortex and antivortex are separated by a large distance, one would expect to see single-vortex voltage steps again. This does not occur for the system size that we considered due to the long range of the interaction. In section 3.2 we considered models for a single vortex; here we consider a model for a pair. We model the vortex–antivortex interaction as being logarithmic. In addition we have to take into account the periodic boundary condition along the y-direction: the vortex can see an antivortex behind it and in front of it (and vice versa). We denote the position of the vortex by y_1, and that of the antivortex by y_2. Let the coordinates take the values $0 \leqslant y_i < L_y$. The images are then at $y_i \pm L_y$. We only take the direct interaction and the interaction of the nearest image charge into account (i.e. at a distance less than L_y). The only stable current-driven pairs in the simulation are the ones that move at a fixed separation Δx; we therefore fixed the separation Δx in this model. This leads to the following equation of motion:

$$\eta(\dot{y}_1)\dot{y}_1 = +i(t) - i_d \sin(2\pi y_1) - \frac{y_1 - y_2}{\Delta x^2 + (y_1 - y_2)^2} + \epsilon \frac{L_y - |y_1 - y_2|}{\Delta x^2 + (L_y - |y_1 - y_2|)^2}$$

$$\eta(\dot{y}_2)\dot{y}_2 = -i(t) - i_d \sin(2\pi y_2) + \frac{y_1 - y_2}{\Delta x^2 + (y_1 - y_2)^2} + -\epsilon \frac{L_y - |y_1 - y_2|}{\Delta x^2 + (L_y - |y_1 - y_2|)^2}.$$

Here ϵ is the sign of $y_1 - y_2$. We have computed the I–V characteristics using these equations and we did indeed find steps at $V = nL_y/m2\pi v$. To capture the mechanism for the pair steps in the model, we found the essential ingredients to be the interaction and the restriction of y_i to L_y—that is, periodic boundary conditions in the y-direction. The detailed form of the interaction determines the bias currents for which the steps occur.

4.2. Defects in a fully frustrated $f = \frac{1}{2}$ array

It was found in [13, 17] that the I–V characteristic of a single excess vortex in a dc-driven $f = \frac{1}{2}$ array resembles that of single vortex in the $f = 0$ case up to a current of $i_{dc} = 0.34$. At the latter current the entire checkerboard of vortices depins, producing a voltage that is much larger than the single-vortex response. The excess vortex moves in an even more non-linear viscous fashion than in the $f = 0$ case [17].

Now we include an ac component in the dc driving current, and we find steps at $V = 2n(2\pi v)$. The factor of two can be explained using the scenario proposed in [28]: first the excess vortex pushes the vortex in front of it to jump, and then follows suit. In total two jumps have been performed. Small subharmonic $V = n(2\pi v)$ ($n = 1, 3$) steps can be distinguished in the I–V characteristic shown in the inset of figure 9.

We find that the I–V characteristic of an excess vortex and a missing vortex (with respect to the checkerboard vortex lattice ground state) in the $f = \frac{1}{2}$ case is similar to that of a vortex and an antivortex respectively in the $f = 0$ case. An excess vortex can be annihilated by a missing vortex. We calculated the I–V characteristic for different values of Δx. In these I–V characteristics one again finds the fractional vortex–antivortex-pair steps as in the $f = 0$ case. One observes in figure 9 that as the separation Δx becomes larger, these steps disappear, and the steps corresponding to single vortices grow, as one would intuitively expect. Finally only the latter remain.

5. Summary and discussion

In this paper we have discussed the phase-locking behaviour of a single vortex and a vortex–antivortex pair under the influence of an ac + dc drive. We obtained harmonic and

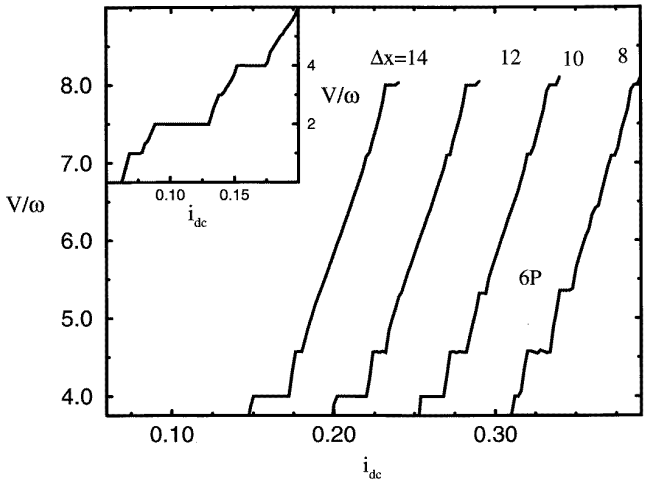

Figure 9. I–V characteristics obtained by driving an excess and a missing vortex, separated by Δx, in the vortex lattice of an overdamped fully frustrated 32×32 array. The ac component has frequency $\nu = \frac{1}{25}$ and amplitude $i_{ac} = 0.10$. The curves are plotted for the separations $\Delta x = 8$, 10, 12, 14. In the inset we show an I–V characteristic of an extra vortex moving in the ground-state vortex lattice of the fully frustrated 16×16 array. The frustration is $f = \frac{1}{2} + \frac{1}{15 \times 16}$, and $i_{ac} = 0.10$, $\nu = \frac{1}{50}$, and $\beta_c = 0$.

subharmonic single-vortex voltage steps, and studied the microscopic vortex dynamics. We found period-doubled vortex motion. The $n = 1$ step corresponds to a vortex jumping one plaquette per period, since in a periodic array all of the plaquettes in the same column along the periodic direction are equivalent, and one would expect period-one behaviour. The simulation, in which period-doubling vortex motion is observed, was performed in an 8×8 array with $\beta_c = 25$. In this case the vortex motion can excite spin waves [13, 14]. These spin waves cause a spatially modulated environment for the vortex. Similar phase-locking is observed in a ring of Josephson junctions [27].

The spin waves may also be responsible for the complicated behaviour of the hysteresis that we observed in (ac + dc)-driven arrays as a function of β_c. In recent experiments subharmonic giant Shapiro steps [3] were observed in over- and underdamped arrays. In simulations it was shown that one can have such steps in a 2-D array by either including disorder [6] or inductive effects [7], or generally any mechanism that breaks the translational invariance of the array. In overdamped single junctions one can only get subharmonics by using non-sinusoidal current-phase relationships [26]. Our simulations show that a single vortex itself may phase-lock on subharmonic steps. The simulation of the pair case shows that single-vortex voltage steps are replaced by fractional steps, which can be understood in terms of vortex interaction. Unfortunately this insight also makes it manifest why generalization to the dynamics associated with Shapiro steps that involve many vortices (such as the axisymmetric coherent vortex states) is not feasible. Another consequence of the fact that we find subharmonic steps is that a more realistic vortex equation of motion (than equation (10) and (11)) should contain higher-harmonic corrections to the sinusoidal potential. The presence of higher harmonics in the potential experienced by vortices was already noted by Lobb *et al* [9]. We have shown that the parameters for which single-vortex voltage steps can be observed are within the reach of present-day experiments.

Acknowledgments

We thank D Domínguez, U Geigenmüller, A van Otterlo and A van Oudenaarden for discussions. This work was supported in part by the Dutch organization for fundamental research (FOM). The work of JVJ has been partially supported by NSF grant No DMR-9521845. TJH thanks the Bavarian 'FORSUPRA' programme for financial support.

Note added in proof. After completion of this work we learned from J J Mazo that a similar type of single-vortex or particle-induced step in the I–V characteristics were found in a one-dimensional driven Frenkel–Kontorova model [29, 30]. We thank him for bringing this work to our attention.

References

[1] Clark T D 1973 *Phys. Rev.* B **8** 137
Leeman C, Lerch P and Martinoli P 1984 *Physica* B **126** 475
[2] Benz S P, Rzchowski M S, Tinkham M and Lobb C J 1990 *Phys. Rev. Lett.* **64** 693
[3] Lee H C, Newrock R S, Mast D B, Hebboul S E, Garland J C and Lobb C J 1991 *Phys. Rev.* B **44** 921
Hebboul S E and Garland J C 1991 *Phys. Rev.* B **43** 13 703
[4] Lee K H, Stroud D and Chung J S 1990 *Phys. Rev. Lett.* **64** 962
Free J U, Benz S P, Rzchowski M S, Tinkham M and Lobb C J 1990 *Phys. Rev.* B **41** 7267
Lee K H and Stroud D 1991 *Phys. Rev.* B **43** 5280
Octavio M, Free J U, Benz S P, Newrock R S, Mast D B and Lobb C J 1991 *Phys. Rev.* B **44** 4601
[5] Yu W, Harris E B, Hebboul S E, Garland J C and Stroud D 1992 *Phys. Rev.* B **45** 12 624
[6] Domínguez D, José J V, Karma A and Wiecko C 1991 *Phys. Rev. Lett.* **67** 2367
Domínguez D and José J V 1993 *Phys. Rev.* B **48** 13 717
[7] Domínguez D and José J V 1992 *Phys. Rev. Lett.* **69** 514
Phillips J R, van der Zant H S J, White J and Orlando T P 1994 *Phys. Rev.* B **50** 9387
[8] Benz S P and Burrough C J 1991 *Appl. Phys. Lett.* **58** 2162
[9] Lobb C J, Abraham D W and Tinkham M 1983 *Phys. Rev.* B **27** 150
[10] Eckern U and Schmid A 1989 *Phys. Rev.* B **39** 6441
Eckern U 1990 *Applications of Statistical and Field Theory Methods to Condensed Matter (NATO Advanced Studies Institute, Series B: Physics, vol 218)* ed D Baeriswyl *et al* (New York: Plenum) p 311
Rzchowski M S, Benz S P, Tinkham M and Lobb C J 1990 *Phys. Rev.* B **42** 2041
Orlando T P, Mooij J E and van der Zant H S J 1991 *Phys. Rev.* B **43** 10 218
Eckern U and Sonin E B 1993 *Phys. Rev.* B **47** 505
[11] van der Zant H S J, Fritschy F C, Orlando T P and Mooij J E 1990 *Physica* B **165+166** 969
van der Zant H S J, Muller C J, Geerligs L J, Harmans C J P M and Mooij J E 1988 *Phys. Rev.* B **38** 5154
van der Zant H S J, Fritschy F C, Orlando T P and Mooij J E 1991 *Phys. Rev. Lett.* **66** 2531
van der Zant H S J, Fritschy F C, Orlando T P and Mooij J E 1993 *Phys. Rev.* B **47** 295
Tighe T S, Johnson A T and Tinkham M 1991 *Phys. Rev.* B **44** 10 286
[12] van der Zant H S J, Fritschy F C, Orlando T P and Mooij J E 1992 *Europhys. Lett.* **18** 343
[13] Bobbert P A 1992 *Phys. Rev.* B **45** 7540
Geigenmüller U, Lobb C J and Whan C B 1993 *Phys. Rev.* B **47** 348
Yu W and Stroud D 1994 *Phys. Rev.* B **49** 6174
[14] Geigenmüller U 1997 Ballistic vortex motion in Josephson arrays *Preprint*
[15] Yu W and Stroud D 1992 *Phys. Rev.* B **46** 14 005
[16] Yu W, Lee K H and Stroud D 1993 *Phys. Rev.* B **47** 5906
[17] Hagenaars T J, Tiesinga P H E, van Himbergen J E and José J V 1994 *Phys. Rev.* B **50** 1143
Hagenaars T J, Tiesinga P H E, van Himbergen J E and José J V 1995 *Quantum Dynamics of Submicron Structures (NATO Advanced Studies Institute, Series E: Applied Sciences, vol 291)* ed H A Cerdeira *et al* p 617
[18] See for instance
Likharev K K 1986 *Dynamics of Josephson Junctions and Circuits* (Philadelphia, PA: Gordon and Breach) and references therein
[19] Hagenaars T J, van Himbergen J E, José J V and Tiesinga P H E 1996 *Phys. Rev.* B **53** 2719
[20] McCumber D E 1968 *J. Appl. Phys.* **39** 3113

Stewart W C 1968 *Appl. Phys. Lett.* **12** 277
[21] Shapiro S 1963 *Phys. Rev. Lett.* **11** 80
[22] Eikmans H and van Himbergen J E 1990 *Phys. Rev.* B **41** 8927
[23] Eikmans H and van Himbergen J E 1992 *Phys. Rev.* B **45** 10 597
[24] These parameters are for arrays fabricated at Delft Technical University by A van Oudenaarden. The bias current I_{dc} can be measured with an accuracy of $\Delta I = 10^{-9}$ A, the voltage V with an accuracy of $\Delta V = 10^{-7}$ V. The feasible frequency range is $\nu = 1$–10 MHz.
[25] Greenside H S and Helfand E 1981 *Bell Syst. Technol. J.* **60** 1927
[26] Renne M J and Polder D 1974 *Revue Phys. Appl.* **9** 25
Lübbig H and Luther H 1974 *Appl. Rev. Phys.* **9** 29
[27] van der Zant H S J, Orlando T P, Watanabe S and Strogatz S H 1995 *Phys. Rev. Lett.* **74** 174
[28] Dang E K F and Györffy B L 1993 *Phys. Rev.* B **47** 3290
[29] Mazo J J *et al* 1995 *Phys. Rev.* B **52** 6451
[30] Floria L M and Mazo J J 1996 *Adv. Phys.* **45** 505